Magnetization reversal and wall propagation velocity in single-crystalline and polycrystalline Fe wires

Y. Kasatani,[1,*,†] A. Yamaguchi,[1,2,*,‡] H. Yamamoto,[1] and H. Miyajima[1,*,§]
[1]*Department of Physics, Keio University, Hiyoshi, Yokohama 223-8522, Japan*
[2]*PRESTO, JST, Honcho, Kawaguchi, Saitama 332-0012, Japan*
(Received 1 April 2010; published 18 June 2010)

The propagation velocities of a magnetic domain wall (DW) in polycrystalline and single-crystalline layers of Fe(001)/Au/$Fe_{19}Ni_{81}$ wires were measured using the giant magnetoresistance effect. In a single-crystalline Fe wire, the DW propagation velocity (1 km/s in a 110 Oe field at 77 K) was about three times faster than that in a polycrystalline Fe wire. This is attributable to the increase in an effective damping derived from incoherent rotation of the magnetization, which reduced the DW's mobility in the polycrystalline wire. Magnetocrystalline anisotropy plays an important role in the nucleation of DW and the switching process. Analytic solutions for the DW's motion have been found on the basis of an approximation suggested by the Slonczewski-Walker and Becker-Döring models; these solutions can explain our experimental results.

DOI: 10.1103/PhysRevB.81.224425 PACS number(s): 75.60.Ch, 75.47.De, 75.78.Fg, 81.07.Gf

Artificial low-dimensional magnetism has stimulated the discovery of phenomena in thin films and multilayers, and suggested the potential application of thin-films systems to magnetic storage media and sensor technology. An important property of this magnetism is the unusual magnetic switching processes it displays. When the sample sizes are reduced to dimensions comparable to the relevant physical length, such as the domain-wall (DW) width or the exchange length, questions arise concerning the stability of the static magnetic state and the magnetic switching characteristics. In such systems, the effects associated with the sample edges influence the magnetization state in small magnetic elements. Local symmetry-breaking structures related to the magnetization reversal process, such as edge and grain boundaries have been relevant. In contrast, under epitaxial growth conditions, the magnetocrystalline anisotropies are very well defined across the entire crystal, and strong exchange coupling between atomic layers inhibits any variations in magnetization across the thickness of the film to the first order. Thus, the single-crystalline magnet is greatly simplified and, therefore, is an excellent system for studying fundamental magnetic phenomena. Investigation of the magnetic switching characteristics in small magnetic elements with single-crystalline properties provides a fundamental scientific understanding. Small magnets are promising candidates for investigating fundamental magnetism and for use in spintronic applications.

Magnetic switching is the process by which an applied field is used to change the direction of magnetization. Such changes are usually mediated by DW displacement. Many studies of DW dynamics and the propagation velocity of a DW have been performed.[1–12] One important study concerns the experimental observation of Walker breakdown,[3] which is marked by a region of negative differential mobility and highly irregular wall motion in a ferromagnetic wire, using Kerr microscopy[10] and the tunneling magnetoresistance effect.[11] Studies of single DW dynamics have been performed using a soft ferromagnetic material, permalloy ($Fe_{20}Ni_{80}$ or $Fe_{19}Ni_{81}$), with negligible magnetic crystalline anisotropy and a polycrystalline structure.[6–11] Even in the most idealized cases, exact integration of the DW propagation equations is very difficult, mainly due to their nonlinear character, derived from the time evolution of internal structural changes in the moving DW.[3] This is also influenced by the magnetic pinning effect arising from the enhanced relative contributions of segregated phases, grain boundaries, and edge roughness.[8]

One important factor affecting DW dynamics is magnetic anisotropy, which consists of magnetic shape anisotropy and magnetocrystalline anisotropy.[3] Although DW propagation in polycrystalline wires has been studied experimentally, single DW propagation in a single-crystalline Fe wire with controlled magnetocrystalline anisotropy has not been investigated. Thus, as described above, while many studies have examined permalloy elements, which are characterized by a small magnetic anisotropy, only a few investigations have been performed for materials with strong magnetic anisotropy.

In this paper, we studied DW propagation in single-crystalline Fe wires using the noncoupled-type giant magnetoresistance (GMR) effect,[6] which is a change in electrical resistance arising from a change in magnetic structure. The method provides sensitive electrical detection of magnetic structural changes in a three-layer ferromagnetic/nonmagnetic/ferromagnetic wire through resistance measurements. The GMR change in the wires is directly proportional to the length of the switching layer magnetization. Therefore, we can determine the position of the DW in the wire by measuring the resistance and estimate the DW's propagation velocity by measuring the time variation of the resistance during magnetization reversal. We explored the poly and single-crystalline-dependent dynamics of DWs in Fe wires.

A high-quality single-crystalline $Fe(001)_{bcc}$ layer on a MgO(001) substrate and a polycrystalline Fe layer on a thermally oxidized Si substrate were prepared in ultrahigh vacuum (UHV) by electron-beam evaporation.[13,14] The base pressure during growth was kept at 10^{-8} Pa. Au(10 nm)/$Fe_{19}Ni_{81}$(10 nm) were then deposited, followed by 3-nm-thick protective Au cap on the Fe layer of interest to this study, at room temperature using electron-beam evapo-

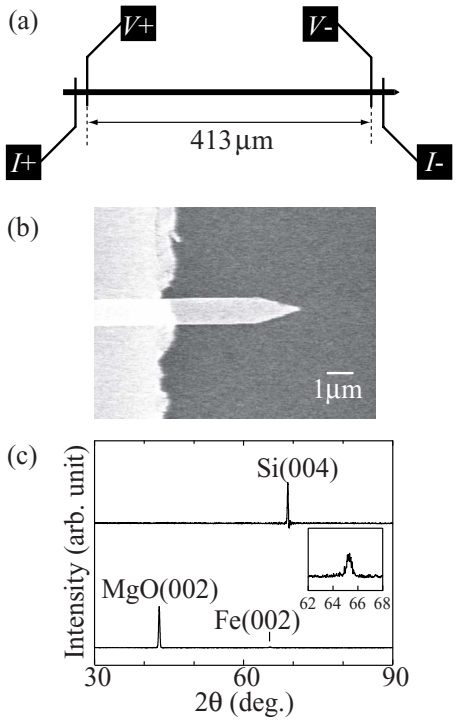

FIG. 1. (Color online) (a) Schematic of the wire with the electrode terminals, (b) SEM image of the sharpened end of the wire, and (c) thin-film XRD spectra of $Fe/Au/Fe_{19}Ni_{81}$ deposited on a thermally oxidized Si substrate and single-crystalline $Fe/Au/Fe_{19}Ni_{81}$ deposited on a MgO(001) substrate. Inset in (c) is a magnification of the spectrum of $Fe(002)_{bcc}$.

ration in UHV. We fabricated 1-μm-wide wires using electron-beam lithography and Ar ion milling.[15] Electrodes were made by patterning Cr (3 nm)/Au (100 nm) films. Schematic and scanning electron microscope (SEM) images of a typical wire are shown in Figs. 1(a) and 1(b), respectively. The voltage electrodes are 413 μm apart. One end of the wire is tapered to a sharp point to prevent nucleation of the DW and ensure that the DW is injected only from the blunt edge of the wire. The structure was characterized by reflection high-energy electron diffraction (RHEED) and x-ray diffraction (XRD) measurements. The RHEED image of the Fe surface (not shown) indicates good crystal orientation of $Fe(001)_{bcc}$ and good flatness. Because no halo reflection pattern from Fe-O was observed, we know that the Fe layer, evaporated in UHV by an adequately outgassed Fe source, was not oxidized. The XRD result is shown in Fig. 1(c). Only the (00n) diffraction peaks are observed, indicating that the film is strongly textured in the (001) planes and is epitaxially grown on the MgO substrates. $Au(10\ nm)/Fe_{19}Ni_{81}(10\ nm)/Au(3\ nm)$ layers were deposited on the Fe layer at room temperature using electron-beam evaporation. Three types of wire systems were prepared: epitaxial $Fe(001)[100]_{bcc}/Au/Fe_{19}Ni_{81}$, $Fe(001)[110]_{bcc}/Au/Fe_{19}Ni_{81}$, and polycrystalline $Fe/Au/Fe_{19}Ni_{81}$, hereafter called [100] wire, [110] wire, and polywire, respectively.

A magnetic field H was applied along the axis of the wire and the resistance R was determined using a standard four-point dc technique at 77 K. Representative magneto-

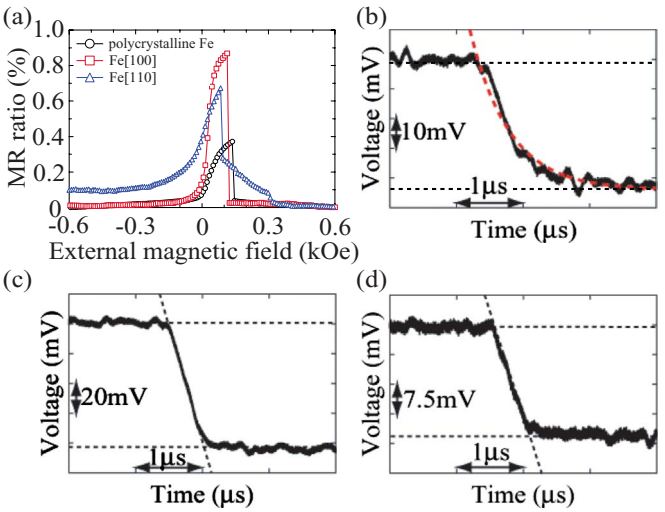

FIG. 2. (Color online) (a) Change in magnetoresistance observed at 77 K. Time variation of the resistance during magnetization reversal at 77 K in (b) polywire (c) [100] wire, and (d) [110] wire, respectively. Dashed line in Fig. 2(b) denotes the fitting curve described by Eq. (3) for $\eta/\beta = 1.69 \times 10^6\ s^{-1}$.

resistance measurement results are shown in Fig. 2(a). Our previous study[15] showed that in single-crystalline $Fe(001)[110]_{bcc}/Au/Fe_{19}Ni_{81}$ wire, the magnetocrystalline anisotropy forced the magnetization of the pinned $Fe(001)[110]_{bcc}$ layer of the system to tilt from the longitudinal axis of the wire in the absence of the field. The earlier study also showed that the magnetization reversal process correlates well with the DW injection model,[16] in which the effective field pushes the pinned DW from the blunt edge of the wire toward the wire axis. This clearly shows that the resistance at 0 Oe of the [110] wire has already risen and the switching field is lower than the others shown in Fig. 2(a). In addition, after the initial switching at about 80–90 Oe, the resistance gradually decreases with the field. This behavior is attributed to the switching process associated with the magnetocrystalline anisotropy of the Fe layer. As a result of the fourfold symmetry, magnetization reversal as a function of an applied magnetic field occurs by a two-step switching process. When the strength of the applied field along the longitudinal axis of the wire is reduced, the magnetization of $Fe(001)[110]_{bcc}$ rotates from the initial field direction to the nearest axis, the [100] or [010] direction. With further reduction and reversal of the applied field, the magnetization switches irreversibly from the [100] or [010] into the $[\bar{1}00]$ or $[0\bar{1}0]$ direction. With increasing reverse field, the magnetization of the $Fe(001)[110]_{bcc}$ layer finally rotates gradually into the reverse field direction, whereas the magnetization of the $Fe_{19}Ni_{81}$ layer is saturated along the longitudinal axis of the wire in an external field of about 80–90 Oe due to its negligible magnetocrystalline anisotropy.

Next, we measured the time evolution of magnetization reversal in each wire. An electric current in the wire was supplied by a 9 V battery to minimize noise from the current source.[6] The electric current was adjusted using a potentiometer. The voltage across the two voltage probes was monitored by a differential preamplifier and real-time storage

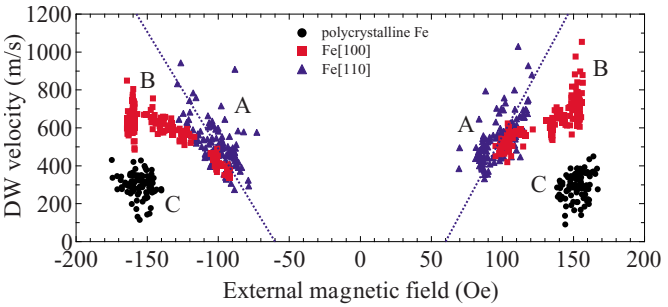

FIG. 3. (Color online) Dependence of DW velocity v on the amplitude of the applied magnetic field H at 77 K.

oscilloscope with a sampling rate of 20×10^9 s^{-1} and bandwidth of 4 GHz. An experimental sequence began with the nucleation of a reversed DW and the associated DW at the nucleation edge by applying a magnetic field along the wire's axis. The time variation in the resistance corresponds to the time variation in the DW's position in the wire because the DW comes from the side of one voltage probe and runs toward the other voltage probe. Therefore, the time variation in the DW position can be estimated by the GMR resistance-measurement method.[6]

Typical results for the time variation in the resistance during magnetization reversal in the polywire, [100] wire, and [110] wire are shown in Figs. 2(b)–2(d), respectively. The linear variation in resistance with time in Figs. 2(c) and 2(d) indicates that the propagation velocities of the DW are constant during magnetization reversal in both the [100] wire and [110] wire, respectively. In contrast, the nonlinear time variation in the resistance in Fig. 2(b) indicates that the DW propagates in viscous media. These results for the time variation in the resistance were measured more than 120 times in one sample. To confirm the reproducibility and increase the sample population, we prepared three or more samples for each wire and measured all of the wires.

The switching fields of the [100] wire, [110] wire, and polywire ranged from 90 Oe to 160 Oe, 60 Oe to 110 Oe, and 140 Oe to 170 Oe, respectively, as the DW velocity measurement was repeated while changing the external magnetic field. The sign of the field in Fig. 3 corresponds to the direction of the external field. The DW velocities increased with increasing field, as shown in Fig. 3, independent of the polarity of the DW, i.e., in head-to-head and tail-to-tail DWs. In the [100] wire, the DW reached a velocity of 1 km/s in a field of 110 Oe at 77 K. Thus, the velocity in the single-crystalline wire is at least three times larger than that in the polycrystalline wire with the same edge roughness. While the velocity range of the single-crystalline wire approaches the speed of sound in pure iron, this is characteristic of the viscous motion regime found in the polycrystalline wire.

The switching field H_{SW} and velocity v are stochastic. As shown in Fig. 3, the distributions of v-H characteristics are separated into groups A, B, and C. Groups B and C are composed of the distribution of v-H characteristics for the [100] wire at the higher switching field and the entire data set for the polywire, respectively, while group A includes the entire data set for the [110] wire and a part of the distribution of v-H characteristic for the [100] wire at the lower switching field. These results are attributable to the precession of magnetization within the DW's motion. We were not able to apply the least-squares method to the data in groups B and C because of the narrow distribution range of the v-H characteristics. For the [110] wire only, we can estimate the mobility from $v=\mu(H-H_{SW})$ and Fig. 3, obtaining about $\mu=13.3$ m/(Oe s) and $H_{SW}\sim60$ Oe for the [110] wire. H_{SW} is considered to be the field below which the DW cannot propagate because of the pinning by structural defects. Because the same preparation for all the samples is common, H_{SW} of the polywire is considered to be as same as that of the single-crystalline wires. Assuming $H_{SW}\sim60$ Oe for the polywire, we can estimate the mobility to be approximately $\mu=2.9$ m/(Oe s).

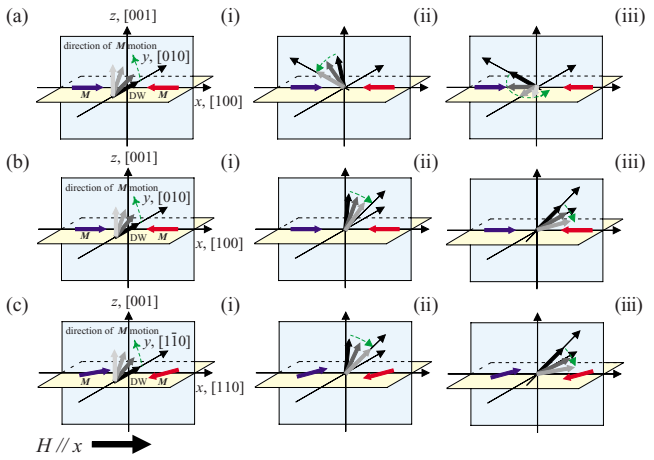

FIG. 4. (Color online) Schematic of time evolution of magnetization reversal routes: (a) (i)–(iii) at the higher switching field in the [100] wire, (b) (i)–(iii) at the lower switching field in the [100] wire, and (c) (i)–(iii) in the [110] wire. Dashed (green) line shows the direction of motion of the magnetization within the DW. Gradated arrows represent the time evolution of the magnetization within DW. The magnetization revolves from the dark arrow direction to the light arrow direction.

Although the shape magnetic anisotropy ($\sim10^6$ J/m^3) is much larger than the magnetocrystalline anisotropy ($\sim5\times10^4$ J/m^3) and is expected to dominate magnetization reversal, the distribution of v-H characteristics for the [100] wire is separated into two groups but that for the polywire is not. According to Cowburn *et al.*[5] and Zhan *et al.*,[14] respectively, the switching between [$\bar{1}$00] and [100] is governed by two separate energy barriers between the hard and easy directions, and the easy directions transit directly through the intermediate direction. Basically, magnetization reversal as a function of an applied magnetic field occurs by a two-jump switching process. Subsequent changes in the orientation of the magnetization during the reversal are indicated by the steps (i)–(iii) in Figs. 4(a)–4(c). The coordinate system in the figures defines the relative orientation between the easy (x) and hard (y,z) shape anisotropy axes and the easy ⟨100⟩ and hard ⟨110⟩ magnetocrystalline anisotropy axes, as well as the direction of the applied field parallel to the longitudinal axis of the wire (x direction). With saturation in the $-x$ direction, the wire is in a single-domain state with the magnetization $\boldsymbol{M}$ aligned parallel to the external magnetic field directed along

the $-x$ direction. With a reduction in the strength of the applied field, the magnetization in the blunt edge of the wire rotates from the initial field direction to the nearest easy axis of the magnetocrystalline anisotropy $\langle 100 \rangle$ in the plane. Thus, the magnetization is almost perpendicular to the wire's axis, which is the easy axis, and a 90° DW is nucleated at the blunt edge. With further reduction and reversal of the applied field along the $+x$ direction, the DW moves quickly to the other edge. On reversal, the magnetization within the DW rotates into the reverse direction through several paths, as shown in Figs. 4(a)–4(c). With an increase in the applied field, the magnetization within the DW rotates from the initial direction [010] or $[0\bar{1}0]$ in the plane to the hard axis [001] out of the plane (parallel to the z axis) [step (i)]. In the magnetization reversal process in the [100] wire, two paths exist from the [001] to the [100] direction via the $\langle 111 \rangle$ and $\langle 110 \rangle$ axes, as shown in Figs. 4(a) and 4(b), respectively. Meanwhile, the magnetization rotates directly from the [001] to the $\langle 100 \rangle$ direction, reversing the initial direction in the plane, as shown in Fig. 4(c) [steps (ii) and (iii)]. In the polywire, demagnetizing fields in the grains become significant; the magnetic moments within an unfavorably aligned domain overcome the magnetocrystalline anisotropy energy and rotate from their original direction to the favorable field direction. The directions of the magnetization within each grain fail to coincide because the exchange coupling between the grains is negligible. Therefore, the demagnetizing field sometimes helps increase the DW's velocity and at other times it helps decrease the velocity. The demagnetizing field is averaged overall and yields the characteristics of the viscous motion regime. This is why the distribution of the DW's propagation velocity in the polycrystalline wire is the smallest.

In a simple theoretical model, the DW's mobility is given by $\mu=(\gamma\Delta/\alpha)$, where Δ and α are the DW's width and the Gilbert damping constant for $H<H_{\mathrm{W}}$, and γ is the gyromagnetic ratio. Here, the DW's width should be given by $\Delta=\sqrt{A/K}$, where A and K are the stiffness constant and magnetic anisotropy energy, respectively.[3,4,9] The Walker field H_{W} can be written as $H_{\mathrm{W}}=\alpha N M_{\mathrm{S}}$, where M_{S} is the saturation magnetization and N is the demagnetizing factor. For $H \gg H_{\mathrm{W}}$, the periodic torque terms tend to average out and the mobility is given by $\mu=\gamma\Delta/(\alpha+\alpha^{-1})$. In the steady region, the Walker model gives a quantitative explanation; however, the model provides a qualitative rather than a quantitative explanation of the slope of v-H in a magnetic wire or any other system for $H \gg H_{\mathrm{W}}$. This information is insufficient for drawing conclusions about the dissipation given by α. For $H \gg H_{\mathrm{W}}$, the DW's motion accompanies the spin-wave generation and enhances the dissipation. The introduction of the effective damping constant α_{eff} enables us to rewrite the mobility as $\mu=\gamma\Delta/\alpha_{\mathrm{eff}}$ for $H \gg H_{\mathrm{W}}$. Therefore, we are able to treat the DW's dynamics for $H \gg H_{\mathrm{W}}$ as well as the rigid DW dynamics for $H<H_{\mathrm{W}}$, as a linear flow regime in which the DW's propagation velocity is proportional to the field.[9,12,17]

On the basis of this description, we estimate the effective damping constant α_{eff} using $\alpha_{\mathrm{eff}}=\gamma\Delta/\mu$. Considering that $\mu=13.2$ m/(s Oe) for the [110] wire and $\mu=2.9$ m/(s Oe) for the polywire, we estimate $\alpha_{\mathrm{eff}}=0.0194$ and 0.0883, respectively. Our measured values for the Gilbert damping factor α, determined by broadband ferromagnetic resonance (FMR) measurements,[18] are $\alpha=0.0345$ and 0.0804 for the [110] wire and polywire with the same width and thickness, respectively.[19] In the polywire, the effective damping factor based on estimation of the DW's velocity is almost the same as the Gilbert damping factor determined by the FMR measurements. This indicates that grains, grain boundaries, and edge roughness do not cause substantial dynamic dissipation in the polywire. The enhancement of the Gilbert damping factor α for the single-crystalline wire is larger than that for the polycrystalline wire. This is attributable to the energy dissipation derived from spin-wave excitation, including several excitation modes revealed by the FMR measurements.[18,19]

From these two linear flow regimes, we are inclined to accept the relation $v \propto H$, corresponding to precessional motion for both $H<H_{\mathrm{W}}$ and $H \gg H_{\mathrm{W}}$. To deal with the pinning effect simply and intuitively, we describe the DW's dynamics using the Becker-Döring model extended by Galt,[2] rather than the Walker model.[3,4] The two models are in agreement in the region where $v \propto H$.

The dynamic DW profile translates as a whole, and its mass includes the coupling between the position of the wall and the internal degree of freedom, namely, its phase in the rigid-wall approximation. We consider the Cartesian coordinate system and DW propagation along the x axis parallel to the longitudinal axis of the wire, as shown in Fig. 4. Then, the motion of the 180° DW under an external magnetic field H can be derived as the steady-state solution of the phenomenological equation

$$m\ddot{x} + \beta\dot{x} + \eta x = 2M_{\mathrm{S}}(H - H_{\mathrm{SW}}), \tag{1}$$

where x is the displacement of the DW, m is its mass per unit area, β is a parameter measuring viscous resistance, and η is an elastic parameter measuring viscous resistance originating from the potential distribution, such as grain boundaries and magnetocrystalline distribution.

Assuming steady state propagation ($\ddot{x}=0$) and the initial condition $x=0$ at $t=0$, we obtain

$$x(t) = \frac{2M_{\mathrm{S}}(H - H_{\mathrm{SW}})}{\eta}\left[1 - \exp\left(-\frac{\eta}{\beta}t\right)\right] \tag{2}$$

and

$$v(t) = \frac{\mathrm{d}x(t)}{\mathrm{d}t} = \frac{2M_{\mathrm{S}}(H - H_{\mathrm{SW}})}{\beta}\exp\left(-\frac{\eta}{\beta}t\right). \tag{3}$$

Here, β is the parameter measuring viscous resistance arising from power dissipation due to precession and damping of magnetization because of a DW moving with velocity v in an applied field H. According to Galt,[2] $\beta=(\lambda/\gamma^2)\int\sqrt{g(\boldsymbol{r})}/A\mathrm{d}\boldsymbol{r}$, where λ denotes the damping constant in the Landau-Lifshitz equation. The Gilbert damping α enables us to write $\lambda=\alpha\gamma M_{\mathrm{S}}$. $g(\boldsymbol{r})$ is the total anisotropy energy density, consisting of the magnetocrystalline and magnetostatic anisotropy. Here, the DW's width is given by $\Delta=\sqrt{A}/(\int\sqrt{g(\boldsymbol{r})}\mathrm{d}\boldsymbol{r})$. The viscous resistance β can be written as $\beta=\alpha M_{\mathrm{S}}/(\gamma\Delta)$. In the single-crystalline wire, we assume that the DW moves in the

absence of the pinning potential, i.e., when $\eta=0$. Then, the displacement and velocity of the DW are given by $x(t)=2M_S(H-H_{SW})t/\beta$ and $v=2M_S(H-H_{SW})/\beta$, respectively. On the other hand, if the DW is displaced in the polywire, namely, $\eta\neq 0$, the average velocity becomes $\langle v\rangle=2M_S(H-H_{SW})(1-e^{-1})/\beta$ from Eq. (3) for $\eta\to\infty$. The intrinsic mobility μ is given by $\mu=2M_S/\beta=2\gamma\Delta/\alpha$. Here, replacing $\alpha/2$ with the effective damping constant α_{eff}, we obtain $\mu=\gamma\Delta/\alpha_{\text{eff}}$ for the effective mobility. This relation agrees with the Slonczewski and Walker relation $\mu=\gamma\Delta/\alpha_{\text{eff}}$. According to Galt,[2] the energy of the DW's motion, $mv^2/2$, is equal to the dissipation energy in steady DW motion, $[v^2/(2\gamma^2\sqrt{A})]\int\sqrt{g(\boldsymbol{r})}\mathrm{d}\boldsymbol{r}$. Consequently, the DW's mass m is described by $m=(1/\gamma^2\sqrt{A})\int\sqrt{g(\boldsymbol{r})}\mathrm{d}\boldsymbol{r}=\beta/\lambda=1/(\gamma^2\Delta)$. If this conjecture is correct, the DW's mass is determined only by the material and shape of the sample. This enables us to calculate the DW's mass as $m\approx 9.8\times 10^{-8}$ kg/m^2 using only the shape magnetic anisotropy, because the dimension of all wires is the same in our system, and the shape magnetic anisotropy energy is estimated to be $K_u\approx 1.8\times 10^6$ J/m^3, which is much larger than the magnetocrystalline anisotropy energy of Fe $K_1\approx 5\times 10^4$ J/m^3.[20]

Here, we apply Eq. (2) to only the polycrystalline wire and estimate the relaxation time as $\beta/\eta\sim 600$ ns from the fitting in Fig. 2(b). This relaxation time corresponds to the mean free time of the DW's motion.

In conclusion, we have experimentally obtained the velocity-field characteristics of single domain-wall motion in polycrystalline and two single-crystalline wires controlled by the crystalline anisotropy and shape anisotropy. The magnetocrystalline anisotropy plays an important role in nucleating the DW and in switching the magnetization while the edge quality plays only a secondary role. The DW's propagation velocity in the single-crystalline wire is about three times faster than that in the polycrystalline wire. Analytic solutions based on the Slonczewski-Walker model and the Becker-Döring model can explain our experimental results. In a comparison between the Gilbert damping factor estimated by FMR measurements and the effective damping factor estimated by the DW's mobility, the Gilbert damping factor α is enhanced more in the single-crystalline wire than in the polycrystalline wire. This is attributable to the energy dissipation derived from spin-wave excitation, including several excitation modes seen in the FMR measurements. This means that the coherence length in the single-crystalline wires is longer than that in the polycrystalline wire. Assuming a rigid DW model, we estimate the relaxation time corresponding to the mean-free time of the DW's motion in the polywire. These findings are an important step toward a complete microscopic understanding of DW dynamics. They also raise the possibility of controlling the magnetization switching by modifying the energy barriers by using anisotropy or external fields.

The authors thank G. Tatara, Y. Nakatani, and Y. Nozaki for helpful discussions. The present study was partly supported by MEXT Grants-in-Aid for Scientific Research in a Priority Area, a JSPS Grant-in-Aid for Scientific Research and the JST PRESTO program.

*Corresponding author.
†ykasatan@phys.keio.ac.jp
‡yamaguch@phys.keio.ac.jp
§miyajima@phys.keio.ac.jp

[1] H. J. Williams and W. Schockley, Phys. Rev. **75**, 178 (1949).
[2] J. K. Galt, Phys. Rev. **85**, 664 (1952).
[3] N. L. Schryer and L. R. Walker, J. Appl. Phys. **45**, 5406 (1974).
[4] J. C. Slonczewski, Int. J. Magn. **2**, 85 (1972); J. Appl. Phys. **44**, 1759 (1973); **45**, 2705 (1974).
[5] R. P. Cowburn, S. J. Gray, J. Ferré, J. A. C. Bland, and J. Miltat, J. Appl. Phys. **78**, 7210 (1995); R. P. Cowburn, S. J. Gray, and J. A. C. Bland, Phys. Rev. Lett. **79**, 4018 (1997); U. Ebels, A. O. Adeyeye, M. Gester, R. P. Cowburn, C. Daboo, and J. A. C. Bland, Phys. Rev. B **56**, 5443 (1997).
[6] T. Ono, H. Miyajima, K. Shigeto, K. Mibu, N. Hosoito, and T. Shinjo, Science **284**, 468 (1999).
[7] D. Atkinson, D. A. Allwood, G. Xiong, M. D. Cooke, C. C. Faulkner, and R. P. Cowburn, Nature Mater. **2**, 85 (2003).
[8] Y. Nakatani, A. Thiaville, and J. Miltat, Nature Mater. **2**, 521 (2003).
[9] A. Thiaville, J. M. Garcia, and J. Miltat, J. Magn. Magn. Mater. **242-245**, 1061 (2002).
[10] G. S. D. Beach, C. Nistor, C. Knutson, M. Tsoi, and J. L. Erskine, Nature Mater. **4**, 741 (2005).
[11] K. Kondou, N. Ohsima, S. Kasai, Y. Nakatani, and T. Ono, Appl. Phys. Express **1**, 061302 (2008).
[12] P. J. Metaxas, J. P. Jamet, A. Mougin, M. Cormier, J. Ferré, V. Baltz, B. Rodmacq, B. Dieny, and R. L. Stamps, Phys. Rev. Lett. **99**, 217208 (2007).
[13] K. Shikada, K. Tabuchi, M. Ohtake, F. Kirino, and M. Futamoto, J. Magn. Soc. Jpn. **32**, 296 (2008).
[14] Q. F. Zhan, S. Vandezande, K. Temst, and C. VanHaesendonck, Phys. Rev. B **80**, 094416 (2009).
[15] H. Yamamoto, Y. Kasatani, A. Yamaguchi, and H. Miyajima, J. Phys.: Conf. Ser. **200**, 042028 (2010).
[16] E. Kondorski, Phys. Z. Sowjetunion **11**, 597 (1937).
[17] J. Yang, C. Nistor, G. S. D. Beach, and J. L. Erskine, Phys. Rev. B **77**, 014413 (2008).
[18] A. Yamaguchi, K. Motoi, A. Hirohata, and H. Miyajima, Phys. Rev. B **79**, 224409 (2009).
[19] Y. Kasatani, A. Yamaguchi, and H. Miyajima (unpublished).
[20] S. Chikazumi, *Physics of Ferromagnetism* (Clarendon, Oxford, 1997).